# Geometric Frustration of Icosahedron in Metallic Glasses

A. Hirata, L.J. Kang, T. Fujita, B. Klumov, K. Matsue, M. Kotani, A.R. Yavari, M.W. Chen

# Geometric Frustration of Icosahedron in Metallic Glasses

A. Hirata,[1] L. J. Kang,[1] T. Fujita,[1] B. Klumov,[2] K. Matsue,[3] M. Kotani,[1,3] A. R. Yavari,[4,1] M. W. Chen[1,5]*

Icosahedral order has been suggested as the prevalent atomic motif of supercooled liquids and metallic glasses for more than half a century, because the icosahedron is highly close-packed but is difficult to grow, owing to structure frustration and the lack of translational periodicity. By means of angstrom-beam electron diffraction of single icosahedra, we report experimental observation of local icosahedral order in metallic glasses. All the detected icosahedra were found to be distorted with partially face-centered cubic symmetry, presenting compelling evidence on geometric frustration of local icosahedral order in metallic glasses.

Determining atomic structure of amorphous materials has been a long-standing problem, because the lack of long-range translational and rotational symmetry renders it experimentally inaccessible by conventional diffraction methodologies. More than half a century ago, Frank proposed that the icosahedron is the most favorable local order in monatomic metallic liquids (*1*), successfully explaining the feasibility of achieving undercooling to below the melting points. Metallic glasses can often be formed from liquid alloys near eutectic compositions and, in accordance with Frank's proposal, binary liquid eutectic compositions can be generated by introducing icosahedral clusters (*2*). Icosahedral order is thus the most generally accepted description of atomic structures of metallic liquids and glasses (*3*–*14*). From a geometrical viewpoint, icosahedra cannot fill the entire three-dimensional (3D) space, even in disordered systems, without distortion where icosahedral rotational symmetry is partially broken (*15*–*17*). Therefore, the locally preferred icosahedra may not be perfectly consistent with the globally stabilized structure, leading to the theoretical predictions of geometrical frustration of icosahedron (*16*–*19*). Although a number of neutron and x-ray scattering experiments have been performed to elucidate icosahedral order in metallic liquids and glasses (*18*, *20*–*22*), only average structural information can be acquired from 1D diffraction profiles generated by the statistical distribution of coexisting polyhedra with various geometrical distortions in real materials. The direct observation of local icosahedral order is still missing. Consequently, the structure features of local icosahedral order and their correlation with the long-range disorder in glasses and liquids are largely unknown. To overcome the experimental difficulty in detecting local atomic configurations in amorphous materials, we recently developed an angstrom-beam electron diffraction (ABED) method to probe local atomic structure using a ~0.4-nm electron beam (*23*). We use the ABED technique to characterize local icosahedral order in a representative $Zr_{80}Pt_{20}$ metallic glass in which the presence of a large fraction of icosahedra has been predicted by computational simulations (*24*, *25*) and this study (fig. S1).

The amorphous structure of the $Zr_{80}Pt_{20}$ metallic glass was confirmed by spherical aberration–corrected high-resolution transmission electron microscopy (TEM), together with selected-area electron diffraction (fig. S2). To obtain local structural information, we employed the ABED technique with a beam diameter of 0.36 nm (full width at half maximum) to characterize a thin foil of the glass (Fig. 1A). To guide the ABED study, we simulated the characteristic ABED patterns of an ideal icosahedron along five-, three-, and twofold directions (Fig. 1B). A large number of ABED patterns were acquired from the thin edge of the TEM foil. When the specimen thickness is thin enough (~3 to 5 nm), individual polyhedra with an appropriate on-axis orientation can be frequently detected by ABED. However, from these measurements we cannot find any ABED pattern that is completely consistent with the simulated icosahedron patterns shown in Fig. 1B. Instead, the acquired ABED patterns only partially match those of the five-, three-, and twofold orientations (Fig. 1C). This is probably due to distorted icosahedra in which icosahedral order is only partially preserved. We thus simulated five-, three-, and twofold ABED patterns of a typical <0 0 12 0> icosahedron taken from the molecular dynamics (MD) model of the metallic glass (fig. S1B). All icosahedra in the MD model are actually distorted from the ideal icosahedron, in agreement with theoretical and computational predictions (*17*–*19*, *24*, *25*). Figure 1C shows the simulated five-, three-, and twofold ABED patterns of the distorted icosahedron.

[1]WPI Advanced Institute for Materials Research, Tohoku University, Sendai 980-8577, Japan. [2]Joint Institute for High Temperatures, Russian Academy of Sciences, Moscow 125412, Russia. [3]Mathematical Institute, Tohoku University, Sendai 980-8578, Japan. [4]Euronano, SIMAP-CNRS, Institut National Polytechnique de Grenoble, BP 75, 38402 St. Martin d'Heres Campus, Grenoble, France. [5]State Key Laboratory of Metal Matrix Composites, School of Materials Science and Engineering, Shanghai Jiao Tong University, Shanghai 200030, PR China.

*Corresponding author. E-mail: mwchen@wpi-aimr.tohoku.ac.jp

Because the icosahedral symmetry can be only partially retained, the diffraction spot intensities differ considerably from those of the ideal icosahedron. The features of the experimental patterns corresponding to five-, three-, and twofold axes are fairly consistent with the simulated ones in the lengths and angles of diffraction vectors, as indicated by the arrowheads, verifying the existence of distorted icosahedra in the metallic glass (fig. S3).

Although the distorted icosahedra can be detected by ABED, the most common ABED patterns during random diffraction scanning are often very simple and different from the five-, three-, and twofold patterns of icosahedral order. The patterns are basically composed of six nearly symmetrical diffraction spots, as shown in Fig. 2A. To understand the structural origins of the simple ABED patterns, we searched all possible on-axis diffraction patterns of highly frequent polyhedra in the metallic glass predicted by the MD simulation. The simple diffraction patterns were found to originate from the distorted icosahedra, in addition to the well-known five-, three-, and twofold patterns. Figure 2B is a simulated ABED pattern calculated from a distorted <0 0 12 0> icosahedron in which the positions of the 12 coordinated atoms are displaced from those in an ideal icosahedron (Fig. 2C). The incident direction is close to a distorted fivefold orientation (see Fig. 2E). The simulated pattern reproduces well the experimental one in the diffraction vectors (lengths and angles) (Fig. 2, A′ and B′). Note that ABED patterns with the equivalent diffraction vectors cannot be obtained from nonicosahedral clusters (fig. S4). We noticed that this kind of diffraction is also partially similar to that of a face-centered cubic (fcc) structure that is also densely packed with 12 coordinated atoms. Figure 2D shows a [110] diffraction pattern of the fcc structure with six strong spots, which is partially consistent with that of the distorted icosahedron but without the golden-ratio relationship between diffraction vectors. This implies that the distorted part of the icosahedron possesses local fcc-like symmetry.

We investigated the structural similarity between the distorted icosahedron and the fcc cluster. Figure 3A depicts three types of atomic clusters with a coordination number of 12: ideal icosahedron, distorted icosahedron, and fcc cluster. The exact atomic sites where the distorted icosahedron (Fig. 3A, middle) differs structurally from the ideal icosahedron and fcc can be seen. Atoms in the distorted part of the icosahedron can be identified by shifting to fcc coordinates. The distorted icosahedron actually includes icosahedral order and a portion of fcc order (fig. S5), accompanying with the variation of Zr-Pt atomic bond length from 0.277 to 0.347 nm. Separate ab initio calculations (Fig. 3B) verify that the distorted icosahedron has a total energy higher than both the perfect icosahedron and the fcc cluster. This indicates that the distorted icosahedra are in an intermediate state between two densely packed configurations: the ideal icosahedron and the fcc cluster. To confirm that the distorted icosahedron with partial fcc symmetry is representative of the local structure of the Zr-Pt metallic glass, we conducted a bond orientational order analysis based on our MD model containing 12,000 atoms (*6*, *26*). Figure 3C shows a probability distribution function for an invariant $\hat{W}_6$, the most sensitive indicator for icosahedral symmetry, calculated using the averages of spherical harmonics associated with the bond directions (*26*). The values for the ideal icosahedron and the fcc cluster are –0.169754 and +0.013161 (*26*), respectively. The invariant $\hat{W}_6$ of the dominant atomic clusters in the metallic glass is seen to have values in between those of the icosahedron and fcc configurations, suggesting that most local atomic arrangements have an intermediate structure between icosahedron and fcc, which is in agreement with the distorted icosahedron characterized by ABED.

Traditionally, the distortion of icosahedra has been suggested from atomic size disparity of constituent elements and/or kinetic fluctuation during glass formation, giving rise to atomic bonding length variation, as well as atomic scale stress and strain in metallic glasses (*27*, *28*). Nevertheless, different from the indiscriminate geometry variation caused by the chemical and kinetic effects, the distorted icosahedra reported here always possess partial fcc symmetry, indicating that the distortion of icosahedra in the metallic glasses is associated with geometric frustration that derives from the competition between two low-energy states (fcc and icosahedron) with dense atomic packing. The chemical variation and kinetic fluctuation may just provide structural perturbations during the development of the intermediate atomic configuration by preventing the formation of ideal icosahedron and fcc clusters. If each icosahedral cluster is isolated, it would naturally tend to minimize the local energy density by forming the densest and most symmetrical

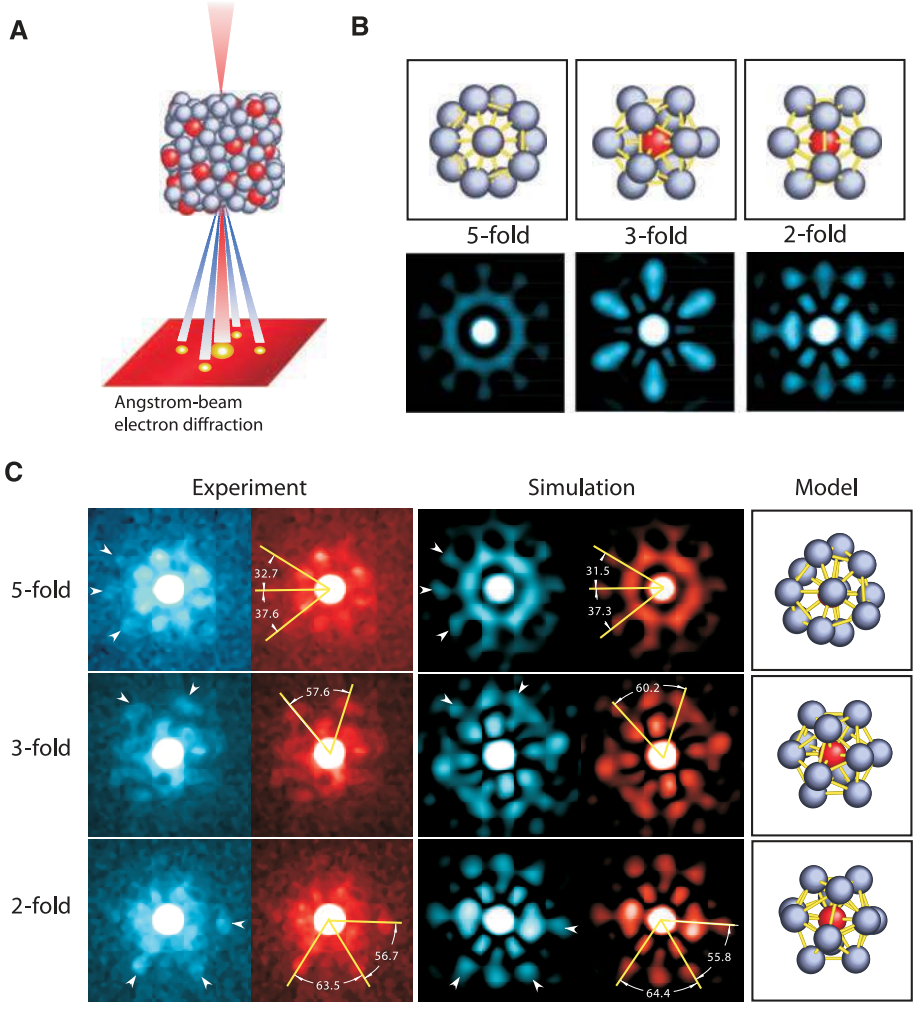


**Fig. 1. ABED characterization of icosahedral order in metallic glasses.** (**A**) Experimental procedure of ABED of a icosahedral cluster. The coherent electron beam has a diameter of 0.36 nm. (**B**) Simulated ABED patterns of an ideal icosahedron. (**C**) Comparison between experimental and simulated ABED patterns of icosahedral clusters in a $Zr_{80}Pt_{20}$ metallic glass. For comparison, angular information between each diffraction vector is shown in the right side of each panel. Arrowheads indicate characteristic diffraction spots of the icosahedral order.

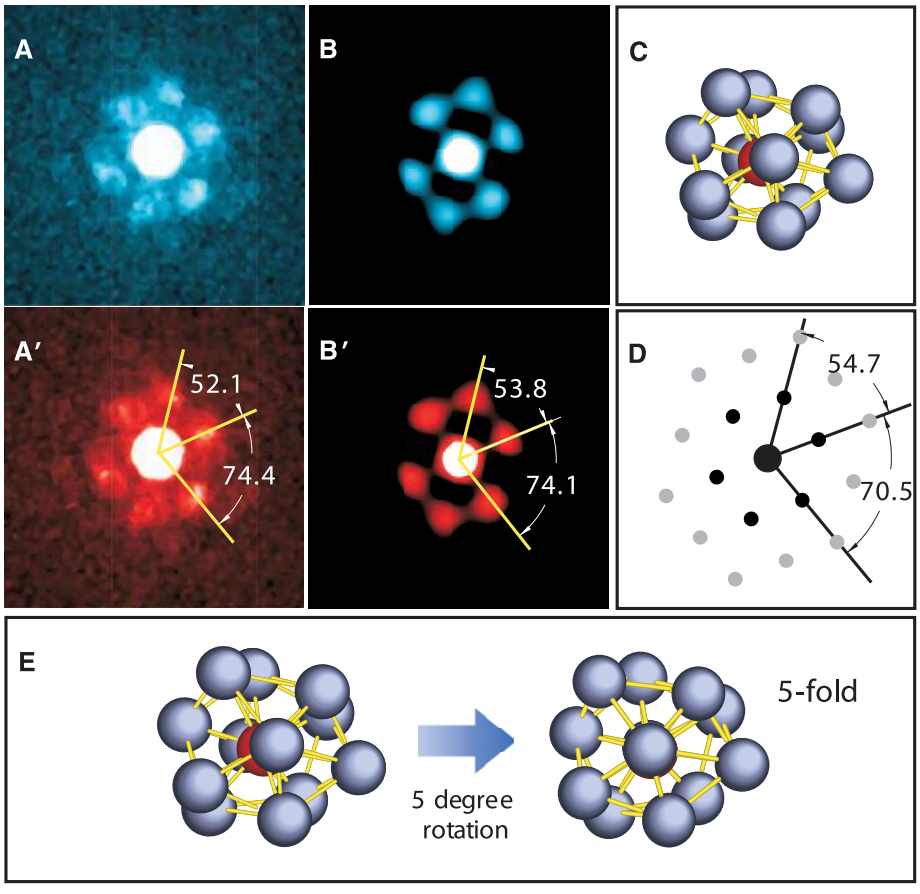


**Fig. 2. ABED patterns of a distorted icosahedron taken from the fcc-like orientation.** (**A**) Experimental ABED pattern with six distinguishable diffraction spots obtained from $Zr_{80}Pt_{20}$. (**A′**) Characteristic diffraction angles in the experimental ABED pattern shown in (A). (**B**) Simulated ABED pattern calculated from the distorted <0 0 12 0> icosahedron taken from the MD model. (**B′**) Characteristic diffraction angles in the simulated ABED pattern shown in (B). (**C**) Illustration of the distorted icosahedron giving the ABED pattern of (B). (**D**) Calculated [110] diffraction pattern of a fcc cluster. (**E**) Correlation between a local fcc symmetry and a distorted pentagon of icosahedral order.

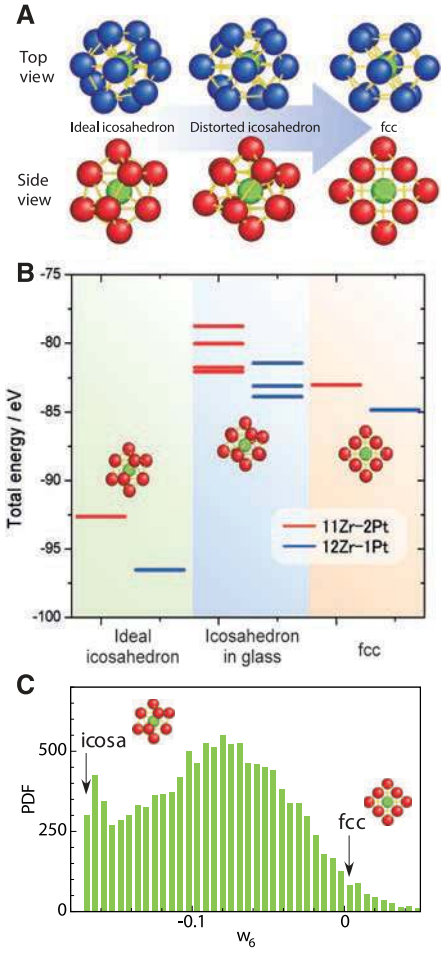


**Fig. 3. Energy calculation and bond orientational order analysis.** (**A**) Structural relationship among the ideal icosahedron, distorted icosahedron, and fcc cluster. (**B**) Total energy calculations of the three atomic clusters. (**C**) Bond orientational order analysis from a 12,000-atom MD model created at a cooling of $10^{10}$ K/s. A histogram of the probability distribution function (PDF) of the $\hat{W}_6$ invariant is shown, together with the characteristic values for an ideal icosahedron and fcc cluster.

icosahedron. However, in real metallic glasses, the constituent atoms shared by neighboring clusters may not always sit at the minima of all pairwise interactions with all of their nearest neighbors, owing to chemical variation and kinetic fluctuation. The fcc symmetry is the energetically and geometrically favorable arrangement of the distorted parts of the icosahedron, because an fcc structure has dense atomic packing with 12 coordinated atoms (same as an icosahedron) and a low energy. Importantly, the local translational symmetry of the fcc configuration makes the distorted icosahedra easy to geometrically match with neighboring clusters for long-range dense packing. Thus, the geometric frustration, evidenced by ABED, reflects the intrinsic structural feature of metallic glasses and correlates with their forming ability and mechanical properties.

It is worth noting that other prevailing clusters in the metallic glass—such as <0 3 6 1>, <0 2 8 0>, <0 2 8 1>, <0 1 10 2>—were also detected by ABED (fig. S6). These clusters also contain both icosahedral- and fcc-like structural features associated with the geometric frustration, similar to the distorted <0 0 12 0> icosahedron. The geometric frustration of the atomic clusters can be quantified by topological analysis. Although each distorted icosahedron or icosahedron-like cluster has distinct geometric distortions depending on the surrounding atomic environment, the preliminary computational homology calculations (*29*), for the first time being applied to the analysis of metallic glasses, show that the geometric distortions of the atomic clusters can be depicted in a simple manner in terms of the topological connectivity. The topological analysis of individual atomic clusters can also be scaled up to long-range disorder (figs. S7 and S8), which may be a promising approach to describe the intricate structure of disordered metallic glasses.

To retain dense atomic packing and a low-energy state, the icosahedral order revealed by ABED is geometrically distorted and inclined to form a mixed configuration, composed of a partial icosahedral symmetry and a partial fcc symmetry. This atomic packing scheme of low structure symmetry but dense atomic arrangement has not been found in any crystal or quasicrystal and represents a distinct atomic structural feature of metallic glasses. Although dominant clusters in metallic glasses are diverse and not limited to icosahedra, dense packing with geometrical frustration appears to be the universal structural characteristic of metallic glass formers.

Metallic glasses are essentially a frozen supercooled liquid. In principle, the local structure revealed by ABED corresponds to the inherent structure of the supercooled liquid immediately before its transition to a glassy state. In addition to shedding light on the structural origins of metallic glass formation, this study also provides evidence that dynamic heterogeneity and arrest in supercooled liquids at the glass transition, as determined from computational simulations and theoretical modeling (*30*–*33*), are essentially associated with local atomic ordering and consequent geometric frustration. Therefore, the ABED experiment may have important implications in

solving the puzzles of glass transition (*34*) and may provide a method to explore the atomic structure and atomic-scale properties of disordered materials.

### References and Notes


1. F. C. Frank, *Proc. R. Soc. London Ser. A* **215**, 43–46 (1952).
2. W. Hume-Rothery, E. Anderson, *Philos. Mag.* **5**, 383–405 (1960).
3. J. D. Bernal, *Nature* **185**, 68–70 (1960).
4. G. D. Scott, *Nature* **194**, 956–957 (1962).
5. J. L. Finney, *Nature* **266**, 309–314 (1977).
6. P. J. Steinhardt, D. R. Nelson, M. Ronchetti, *Phys. Rev. Lett.* **47**, 1297–1300 (1981).
7. T. Tomida, T. Egami, *Phys. Rev. B* **52**, 3290–3308 (1995).
8. M. W. Chen, T. Zhang, A. Inoue, A. Sakai, T. Sakurai, *Appl. Phys. Lett.* **75**, 1697 (1999).
9. D. B. Miracle, *Nat. Mater.* **3**, 697–702 (2004).
10. H. W. Sheng, W. K. Luo, F. M. Alamgir, J. M. Bai, E. Ma, *Nature* **439**, 419–425 (2006).
11. P. F. Guan, T. Fujita, A. Hirata, Y. H. Liu, M. W. Chen, *Phys. Rev. Lett.* **108**, 175501 (2012).
12. D. Ma, A. D. Stoica, X.-L. Wang, *Nat. Mater.* **8**, 30–34 (2009).
13. T. Takagi *et al.*, *Appl. Phys. Lett.* **79**, 485 (2001).
14. A. R. Yavari, *Nat. Mater.* **4**, 2–3 (2005).
15. J. F. Sadoc, R. Mosseri, *Geometrical Frustration* (Cambridge Univ. Press, Cambridge, 1999).
16. D. R. Nelson, *Defects and Geometry in Condensed Matter* (Cambridge Univ. Press, Cambridge, 2002).
17. D. R. Nelson, *Phys. Rev. Lett.* **50**, 982–985 (1983).
18. A. Di Cicco, A. Trapananti, S. Faggioni, A. Filipponi, *Phys. Rev. Lett.* **91**, 135505 (2003).
19. D. R. Nelson, *Phys. Rev. B* **28**, 5515–5535 (1983).
20. T. Schenk, D. Holland-Moritz, V. Simonet, R. Bellissent, D. M. Herlach, *Phys. Rev. Lett.* **89**, 075507 (2002).
21. K. Saksl *et al.*, *Appl. Phys. Lett.* **83**, 3924 (2003).
22. K. F. Kelton *et al.*, *Phys. Rev. Lett.* **90**, 195504 (2003).
23. A. Hirata *et al.*, *Nat. Mater.* **10**, 28–33 (2011).
24. N. A. Mauro *et al.*, *Phys. Rev. B* **83**, 184109 (2011).
25. J. Saida *et al.*, *J. Phys. Condens. Matter* **21**, 375104 (2009).
26. P. J. Steinhardt, D. R. Nelson, M. Ronchetti, *Phys. Rev. B* **28**, 784–805 (1983).
27. T. Egami, S. Aur, *J. Non-Cryst. Solids* **89**, 60–74 (1987).
28. Y. Q. Cheng, E. Ma, *Prog. Mater. Sci.* **56**, 379–473 (2011).
29. T. Kaczynski, K. Mischaikow, M. Mrozek, *Computational Homology* (Springer, New York, 2003).
30. M. D. Ediger, P. J. Harrowell, *J. Chem. Phys.* **137**, 080901 (2012).
31. L. Berthier, G. Biroli, *Rev. Mod. Phys.* **83**, 587–645 (2011).
32. H. Shintani, H. Tanaka, *Nat. Phys.* **2**, 200–206 (2006).
33. G. Tarjus, S. Kivelson, Z. Nussinov, P. Viot, *J. Phys. Condens. Matter* **17**, R1143–R1182 (2005).
34. J. S. Langer, *Phys. Today* **60**, 8–9 (2007).



**Acknowledgments:** We thank Y. Hirotsu and T. Egami for constructive discussion and H. Sheng for providing Zr-Pt embedded atom model potentials and J. Saida for $Zr_{80}Pt_{20}$ ribbons. This work was sponsored by "WPI Research Center Initiative for Atoms, Molecules and Materials," Ministry of Education, Culture, Sports, Science and Technology of Japan; Grants-in-Aid for Scientific Research (24360260 and 24656400), Japan Society for the Promotion of Science; "A mathematical challenge to a new phase of materials science," Japan Science and Technology Agency–Core Research for Evolutional Science and Technology; and the National Natural Science Foundation of China (grant 51271113).

# Supplementary Materials for

## Geometric Frustration of Icosahedron in Metallic Glasses

A. Hirata, L. J. Kang, T. Fujita, B. Klumov, K. Matsue, M. Kotani, A. R. Yavari, M. W. Chen*

*Corresponding author. E-mail: mwchen@wpi-aimr.tohoku.ac.jp

**This PDF file includes:**

## 1. Materials and Methods

### *1-1. Sample preparation and TEM experiment*

$Zr_{80}Pt_{20}$ metallic glass ribbons were made by a single-roll rapid quenching technique with the roll speed of 60 m/sec. The TEM samples were prepared by ion-milling (Fischione, Model 1010) with a liquid nitrogen cooled stage. ABED patterns were taken by using a JEM-2100F TEM/STEM with double spherical aberration (Cs) correctors (operated at 200kV) and recorded by a TV-rate CCD camera (Gatan, ES500W Erlangshen). A nearly parallel coherent electron beam produced by a specially-designed small condenser aperture with a diameter of 5 μm is utilized as an Angstrom-sized electron probe. By using the Cs corrected STEM, the coherent electron beam can be accurately aligned and focused to a diameter as small as 0.3 ~ 0.4 nm and the instrumental parameters (spherical aberration coefficient, defocus, astigmatism etc.) can be precisely measured using a Ronchigram method. (35)

### *1-2. Molecular dynamics calculations and ABED simulations*

*Ab-initio* molecular dynamics (MD) simulation was carried out using the Vienna *ab-initio* simulation package (VASP) (36). The projector augmented wave method (37) and the generalized gradient approximation were used to describe electron-ion interactions (38). A cubic super-cell with a periodic boundary condition and containing 160 Zr atoms and 40 Pt atoms was initially constructed according to the experimental density. The ensemble was melted and equilibrated at a high temperature of 2500 K for 2000 timesteps with the each timestep of 5 fs. Subsequently, the systems were quenched to 300 K with a cooling rate of $4 \times 10^{13}$ K / sec at 1000 time steps per 200 K. All the

calculations were carried out within a canonical ensemble NVT (constant number, volume, temperature) by using a Nosé thermostat for temperature control.

Since a cooling rate of *ab-initio* MD simulation is too high, we also conducted classical MD simulations using embedded atom method (EAM) potentials that were created on the basis of the *ab-initio* calculations. A 12000 atomensemble with the composition of $Zr_{80}Pt_{20}$ was melted at 2500 K for 0.1 ns (with a time step of 5 fs) and then cooled to 300 K at a cooling rate of $1.7 \times 10^{10}$ K/sec.

ABED simulations of the simulated atomic structure were carried out using a conventional multislice method (39). To understand the local atomic environments, we applied Voronoi polyhedral analysis to elucidate possible polyhedra, generally recognized as short range order (SRO), in the metallic glass (Fig. S1A).

## 2. Supplementary Text

### *2-1. Voronoi analysis for the MD model*

In order to interpret the experimental ABED patterns, we investigated the structural model of the glassy $Zr_{80}Pt_{20}$ produced by the *ab-initio* MD simulations and classical MD simulations and applied Voronoi polyhedral analysis to elucidate prevailing polyhedra in the metallic glass. Icosahedron-like polyhedra (<0 1 10 2>) centered by Zr atoms are the dominant SRO and <0 0 12 0> icosahedra are frequently formed around Pt atoms. Figure S1B shows the overall structural model of the *ab-initio* MD simulations, where the central atoms of <0 2 8 1>, <0 0 12 0>, and <0 1 10 2> polyhedra are shown in color. The connections between the colored central atoms indicate the presence of networks consisting of icosahedra and icosahedron-like

polyhedra. Since 167 atoms (total 200 atoms) belong to these three polyhedra, icosahedra and icosahedron-like clusters are apparently the main building blocks of the structural model.

To avoid possible confusion, in this study we define the ideal (or perfect) icosahedron as a <0 0 12 0> cluster with perfect icosahedral symmetry. If the positions of 12-coordinated atoms in a <0 0 12 0> cluster are displaced from those in an ideal icosahedron, we call the clusters as a "distorted" icosahedron. Atomic clusters similar to <0 0 12 0> icosahedra, such as <0 2 8 1> or <0 1 10 2>, which partially contain icosahedral symmetry, are called "icosahedron-like" clusters.

### *2-2. Total energy calculation of individual atomic clusters*

We noticed that the distorted icosahedron observed experimentally is partially analogous to both of the icosahedral and fcc clusters as shown in Fig. 3. To confirm this from the energetic viewpoint, *ab-initio* calculations were performed to estimate the total energies of three types of 11Zr-2Pt and 12Zr-1Pt clusters: ideal icosahedron, distorted icosahedron, and fcc cluster. All the calculations were carried out by using VASP with the projector augmented wave (PAW) method. The generalized gradient approximation (GGA) with Perdew-Burke-Ernzerhof (PBE) exchange-correlation parameterizations was applied. Only the Γ point in Brillouin zone and a supercell with edge length of 16Å were used in the calculations and the energy cutoff is 300eV. The total energies were converged within $10^{-4}$ eV and both structures of the ideal icosahedron and the fcc cluster were relaxed prior to the total energy calculations. The total energy of distorted-icosahedral was directly calculated from the structure obtained by the MD simulations.

### *2-3. Features of atomic clusters other than the <0 0 12 0> icosahedron*

In addition to the <0 0 12 0> icosahedron, we also investigated the prevailing atomic clusters with indices of <0 3 6 1>, <0 2 8 0>, <0 2 8 1>, and <0 1 10 2> in the metallic glasses using ABED. Fig. S6A shows atomic models of the four clusters from two different directions. All the icosahedron-like clusters can be detected in the glass and the corresponding ABED patterns are shown in Fig. S6B and S6C. The experimental diffraction patterns are well consistent with the ones derived from the MD models. As shown in Fig. S6B, the icosahedron-like clusters (<0 2 8 1> and <0 1 10 2>) have very similar ABED patterns to that of the <0 0 12 0> distorted icosahedron. But, the structural difference can be well identified from the ABED patterns. Interestingly all the patterns partially keep the fivefold symmetry whereas only a pair of spots is deviated from fivefold position. Note that the deviated spots consequently make the fcc [110]-like pattern together with the other two pairs of spots. Therefore, both icosahedron- and fcc-like structural features can be identified from the prevailing clusters with indices of <0 3 6 1>, <0 2 8 0>, <0 2 8 1>, and <0 1 10 2>. The concept of geometric frustration can thus be applied to these atomic clusters too, analogous to the <0 0 12 0> distorted icosahedron.

### *2-4. ABED patterns of non-icosahedral clusters in the metallic glass*

The ABED patterns from non-icosahedral clusters such as <0 4 6 3> and <0 3 6 3> were also checked as shown in Fig. S4. The zone-axis patterns obtained from the fivefold-like axes (normal to pentagonal atomic arrangements) are clearly different from the pattern of icosahedra or icosahedron-like clusters. Even by rotating these clusters to

all the possible zone-axis directions, it was impossible to find symmetric patterns similar to the ones obtained from icosahedra.

### *2-5. Topology analysis of atomic clusters in the metallic glass*

In order to survey the manner of distortion of each atomic cluster determined by ABED, we employed a mathematical tool to abstract essence of geometric relations, called “homology group”. Homology groups are defined for geometrical objects called “simplicial complexes” or “cubical complexes”, which are consist of a finite number of simple geometrical objects called n-dimensional simplices (points, segments, triangles, etc.) or cubes (points, segments, squares, etc.), respectively. For given such a complex X and each integer n, the homology group $H_n(X)$ provides the topological feature of X in terms of “n-dimensional holes”. n-dimensional holes may be heuristically thought of as connected components, tunnels and cavities for n=0,1,2, respectively. The homology group $H_n(X)$ can be identified with a $b_n$-dimensional vector space (or a finitely generated module with $b_n$-dimensional free component in algebra). The integer $b_n$ expresses a count of n-dimensional holes in X and is called the n-th Betti number of X, which can be often applied to characterizing the topology of X. For details of the mathematical theory, one can find in the references (29 and 40).

Here we analyze the homology for each atomic cluster in the metallic glass, determined by ABED and MD simulations. The MD model we used in this study consists of 200 atoms, indicating the presence of 200 atomic clusters. For computing homological quantities, we need first to construct three-dimensional objects with voxels (three-dimensional pixels) for the 200 atomic clusters. The voxel dimension is $0.005 \times 0.005 \times 0.005$ nm$^3$. In the case of atoms in metallic glasses, hard sphere model is

basically acceptable. The corresponding cubical complex can be constructed for computing homological quantities. For each atom position in a targeted cluster, we prepared spherical objects with given atomic radii which can be a variable in this analysis. For the computation, we utilized a CHomP (Computational Homology Project) software package available at http://chomp.rutgers.edu/. The CHomP software can provide information of homology, in particular, the Betti numbers, of cubical complexes made by input data such as voxel objects. We here focus especially on the 0-th Betti number $b_0$ which represents the number of connected components in the objects. In the Homology analysis, we always keep the constant inter-atomic distances in the clusters determined by ABED and/or MD simulations while changing the virtual sizes of constituent atoms simultaneously according to their real atomic size ratio, as shown in Fig. S7. For the Zr-Pt binary system, we first determine standard values of atomic sizes which are exactly same as metallic bond radii ($R_A$: 0.16025 nm for Zr; $R_B$: 0.13870 nm for Pt) and always keep the atomic size ratio ($R_A/R_B$) during changing $R_A$ and $R_B$. In this analysis, we use normalized atomic radii that are the virtual atomic radii divided by $R_A$ or $R_B$. The normalized atomic radii of real (or original) atoms are always 1 and the virtual atom size can be larger or smaller than 1. With this simple treatment, we do not need to consider the true atomic sizes during the Homology analysis. Then we can topologically characterize three-dimensional atomic arrangement in the clusters only by one Betti number $b_0$. By changing normalized atomic radii, i.e. monitoring the territory of each atomic coordinate, this method enables us to understand distortion manner for each atomic cluster.

The geometric frustration discussed in this study can also be quantified in terms of its Homology group. The 0-th Betti number $b_0$ can provide the number of

non-connected features in the atomic clusters being analyzed. As shown in Fig. S8, by increasing the atomic radii, the connectivity of the ideal <0 0 12 0> icosahedron changes dramatically from the Betti number 13 (total atom number in the cluster) to 1. Apparently, the distortion caused merely by the atomic size disparity of constituent elements (Pt and Zr) is trivial (Fig. S8). In contrast, the distorted <0 0 12 0> icosahedra determined by ABED show continuous decrease of Betti number from 13 to 1, indicating large variation of inter-atomic distances in the clusters. All the <0 0 12 0> icosahedra in the glass are distorted in the same topological manner and clearly different from the ideal icosahedron. We can scale up the homology analysis from individual atomic clusters to the global structure of the glass to investigate the inherent correlation between local atomic configurations and long-range disordered packing. When we plotted the Betti number variation of the entire MD dataset by counting all the component atoms as centers of polyhedra, we found that the Betti number distribution is consistent with that of the distorted icosahedron and icosahedron-like clusters revealed by ABED. This demonstrates that the connectivity of the distorted icosahedra or icosahedron-like clusters is compatible with the long-range disorder of the metallic glass. Therefore, the homology analysis may provide a simple way to understand the atomic structure of disordered metallic glasses from the topological view.

### *2-6. Detection capability of ABED technique*

Since most TEM specimens are essentially three-dimensional with certain thickness, the volume interrogated by a small electron probe may contain too many atoms to identify the local structure because the sample is too thick. Therefore, for ABED samples, the thinner is better. However, for the TEM samples prepared by ion

milling or electrochemical polishing, the thinnest edge is usually thicker than ~2 - 3 nm. For example, the metallic glass sample used in this ABED study has a thickness of ~3 - 5 nm determined by electron energy loss spectroscopy (EELS). However, even 3 - 5 nm, it is still much thicker compared with the size of individual coordination polyhedra (atomic clusters). We therefore estimated atom numbers inside the column in which electron beam passes thorough by assuming average atomic radii of 0.30 nm and packing density of 0.7. Fig. S9 shows the plots of atom numbers in the column for three different thicknesses (3 and 5 nm). When the beam diameter is focused down to 0.3 ~ 0.4 nm, the atom number is reduced to about 15 ~ 30 atoms, corresponding to 2 ~ 3 atomic clusters. Since the beam diameter is the FWHM value of Gaussian distribution, the actual area that contributes to total ABED intensity is expected to be ~0.5 nm. Nevertheless the atom number is still less than 25 ~ 60 (= 2 ~ 5 atomic clusters) even for the 0.5 nm probe size. Because the ABED intensity strongly depends on the orientation of atomic clusters, it becomes much more realistic to detect a single atomic cluster experimentally using the present ABED technique. We actually checked an effect of the cluster overlapping for the total ABED intensity using the structural models shown in Fig. S10. The simulated ABED pattern is almost unchanged by increasing the number of off-axis cluster. This means only on-axis cluster shows the strong diffraction intensity and gives the main contribution to the total ABED intensity.

We also examined the sensitivity of ABED to the cluster distortion. Fig. S11 shows simulated ABED patterns for both the ideal and distorted icosahedra. The beam incidence direction is slightly tilted from the exact fivefold axis of the clusters. From the exact fivefold axis, the ideal icosahedron only shows a very broad ring (*see* Fig. 1). Even if the cluster is slightly tilted, the pattern still keeps the broadness, clearly different

from the distorted cluster. Moreover, the degree of distortion of icosahedron and icosahedron-like clusters can be determined by ABED. As shown in Fig. S6B, two pairs of diffraction vectors keep at the fivefold positions, but a pair of spots is heavily deviated. The deviation is directly related to the distortion of the clusters. Therefore, using the ABED technique, we can roughly estimate a degree of distortion from the feature of the diffraction patterns.

### *2-7. Atomic structure simulated by a classical MD method (slow cooling)*

Figure S12 shows the results of Voronoi polyhedral analysis from the slowly cooled MD model. The indices of <0 2 8 1>, <0 0 12 0>, <0 2 8 0>, <0 1 10 2>, and <0 2 8 2> are frequently found in the lists. This result is consistent well with the model obtained by our *ab-initio* MD simulation (Fig. S1A). Additionally both of our results are also consistent with the analysis by a reverse Monte Carlo simulation of the identical $Zr_{80}Pt_{20}$ glass (25). We also conducted bond orientational order analysis for the classical MD model as shown in Fig. 3C. Although the statistics of the plot looks much better than that of the *ab-initio* MD model, most of the atomic clusters are situated between ideal icosahedron and fcc.

## 3. Figures

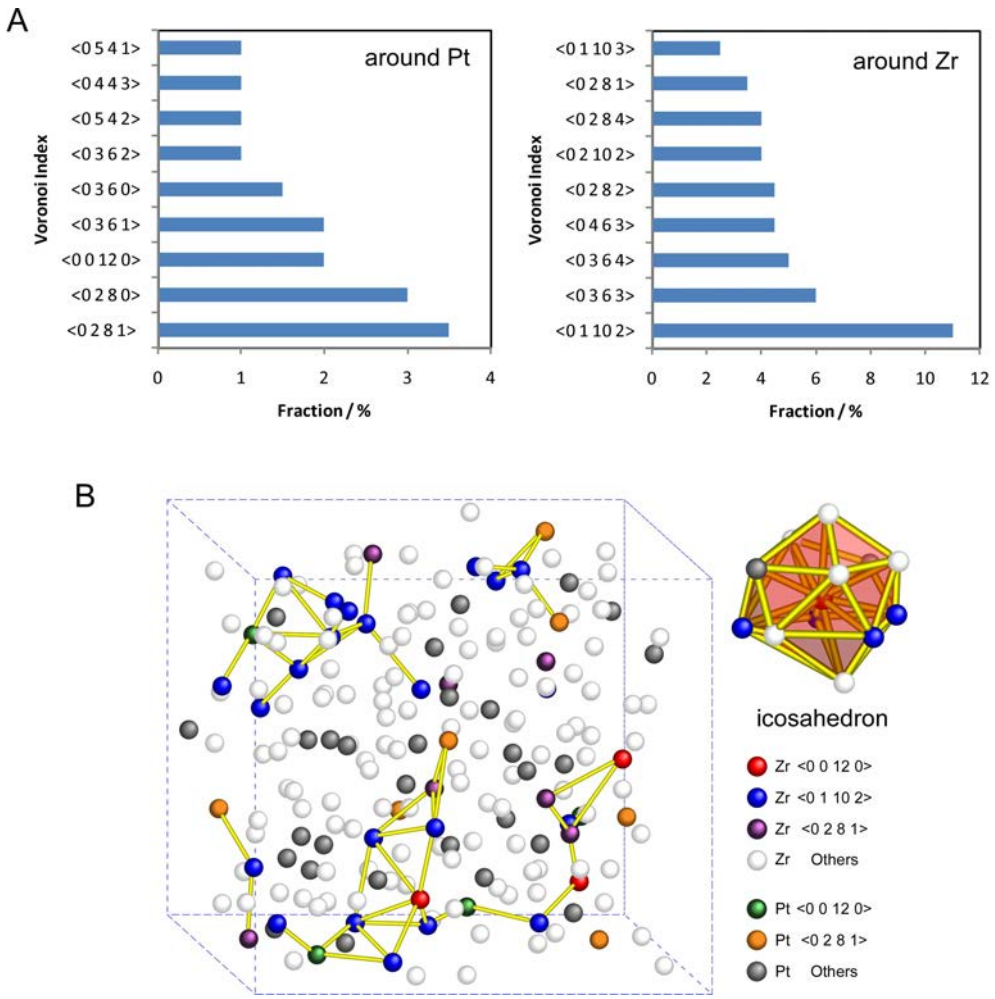


Fig. S1 (A) Voronoi polyhedral analysis of the $Zr_{80}Pt_{20}$ MD structural model. Icosahedra (<0 0 12 0>) and icosahedron-like clusters (<0 1 10 2>, <0 2 8 1>) are frequently observed in the model. The cut-off value for Voronoi analysis is 0.38 nm. (B) Structural model of glassy $Zr_{80}Pt_{20}$ produced by *ab-initio* MD simulation. Colored atoms denote central atoms of icosahedron or icosahedron-like polyhedra. The corresponding Voronoi indices are shown in the inset.

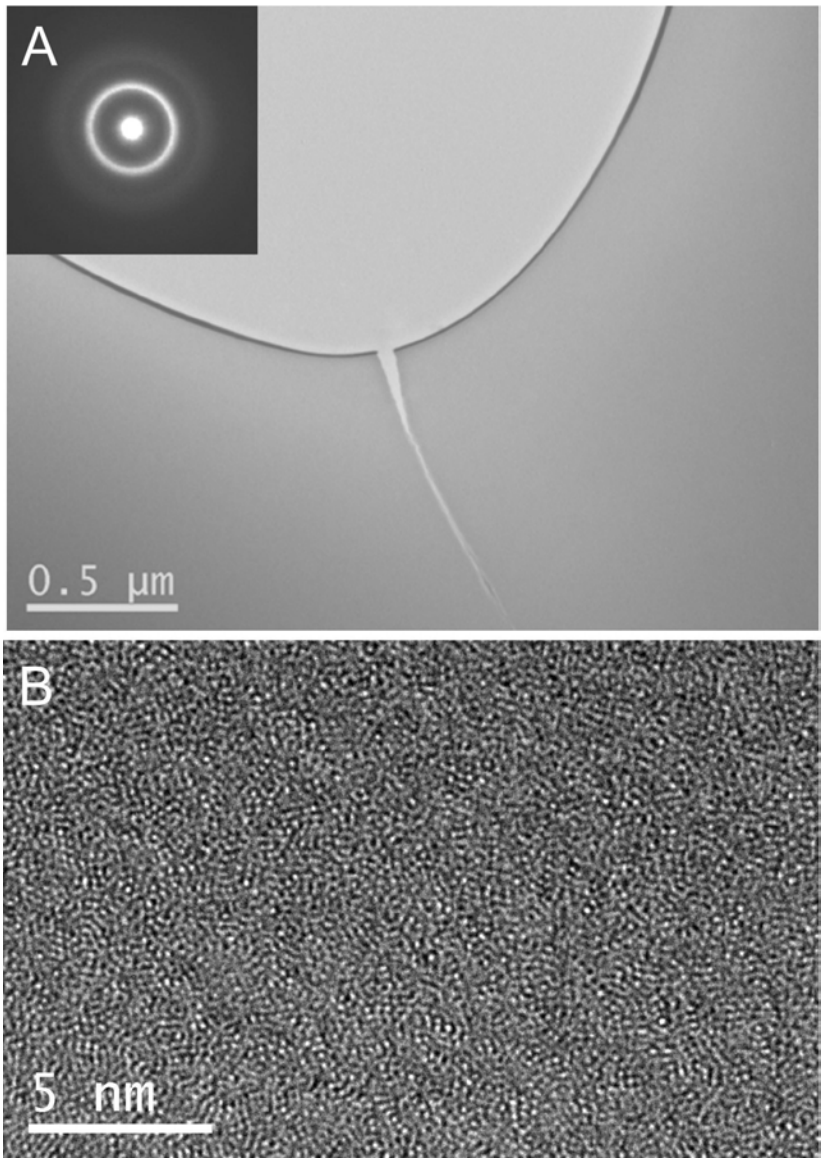


Fig. S2 TEM micrographs of the $Zr_{80}Pt_{20}$ metallic glass. (A) A typical SAED pattern and low-magnification bright-field TEM image; and (B) Spherical aberration-corrected HRTEM image showing the amorphous nature of the sample.

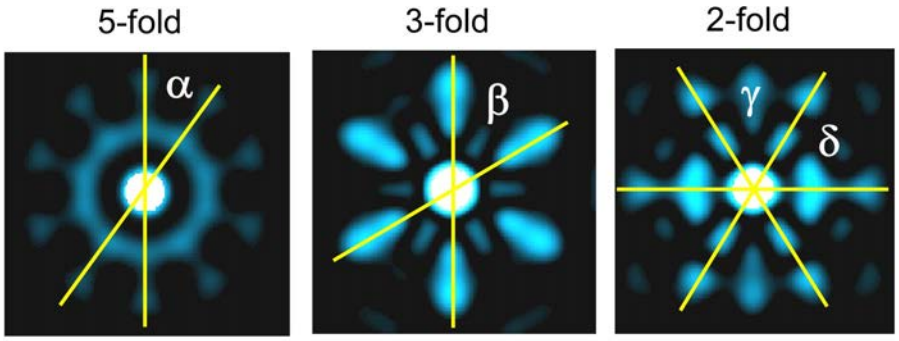


| | α (5-fold) | β (3-fold) | γ (2-fold) | δ (2-fold) |
|---|---|---|---|---|
| Ideal icosahedron | 36.0° | 60.0° | 63.2° | 58.4° |
| Distorted icosahedron | 35.0 ± 3.2° | 60.9 ± 4.2° | 64.8 ± 3.2° | 56.4 ± 9.0° |

Fig. S3 Angular values between two diffraction vectors expected from the ideal and distorted icosahedral clusters. The ranges of the distorted icosahedron are estimated by measuring the angles in several 5-, 3-, and 2-fold patterns obtained from the distorted <0 0 12 0> icosahedral clusters in the MD model. The experimental values shown in Fig. 1C are within the ranges determined from MD models.

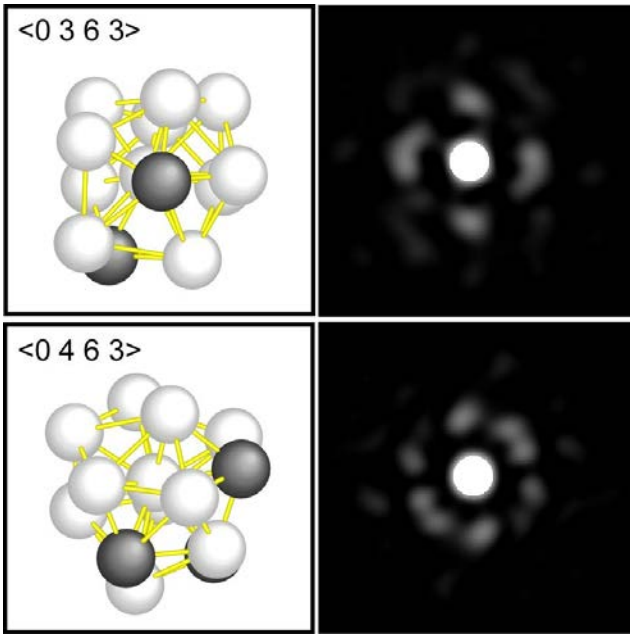


Fig. S4 Simulated ABED patterns from <0 3 6 3> and <0 4 6 3> clusters (non-icosahedral clusters). Although it is difficult to define the fivefold axis in the non-icosahedral clusters, pentagon-like atomic arrangements are roughly normal to the beam incidence in this analysis. The fcc-like pattern seen in the icosahedron cannot be observed in these non-icosahedral clusters.

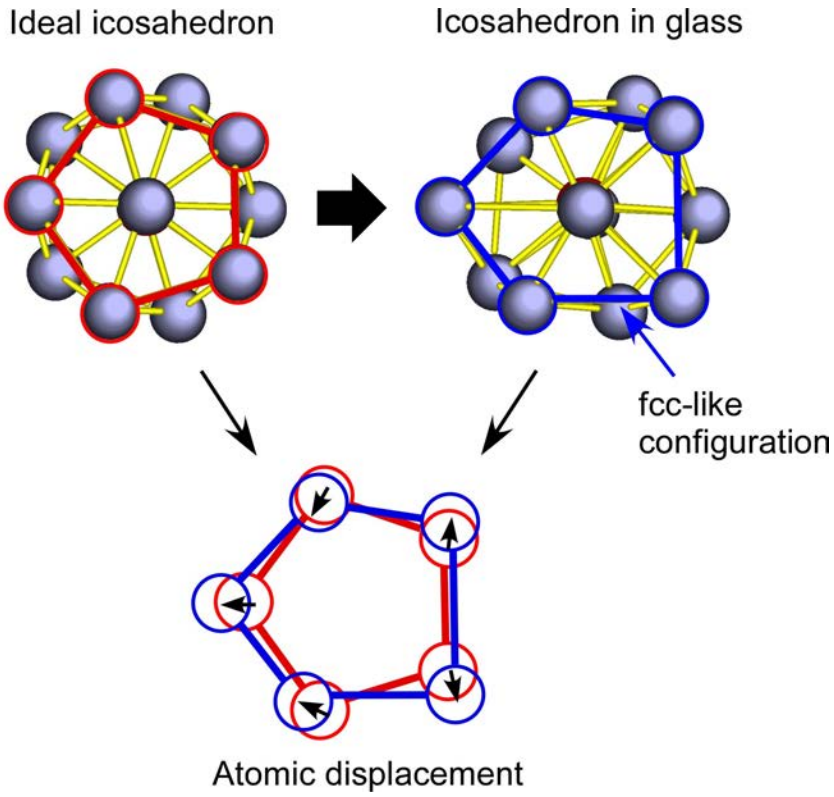


Fig. S5 Structure difference between ideal icosahedrons and the distorted icosahedron detected by the ABED and MD simulations. It can be seen that a pentagon in the ideal icosahedron can turn to be a fcc-like configuration by slight atom shift.

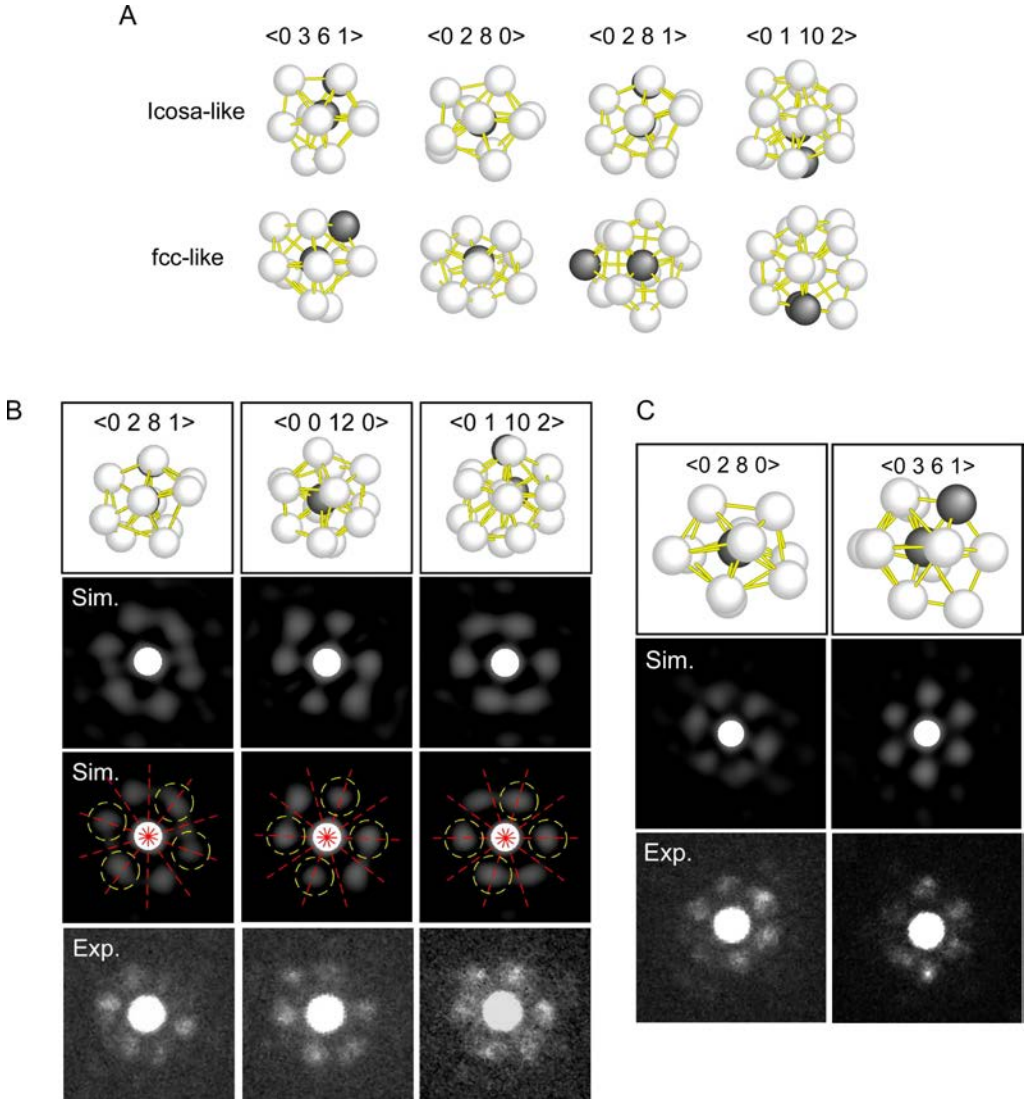


Fig. S6 (**A)** Atomic models of four icosahedron-like clusters that are frequently observed in the metallic glass. Both icosahedron-like fivefold and fcc-like cubic configurations can be recognized from the clusters. (B) Simulated and experimental ABED patterns taken from the distorted icosahedron and icosahedron-like clusters. The beam incidence directions are slightly tilted from the exact fivefold axis. All the patterns partially keep the fivefold symmetry. The diffraction from the distorted portions exhibits a two-fold symmetry, similar to that of the <110> pattern of the fcc cluster. (C) Experimental ABED patterns showing a nearly threefold symmetry, together with the simulated ABED patterns from low-coordination number clusters (<0 2 8 0> and <0 3 6 1>). The simulated patterns are consistent well with the experimental ones.

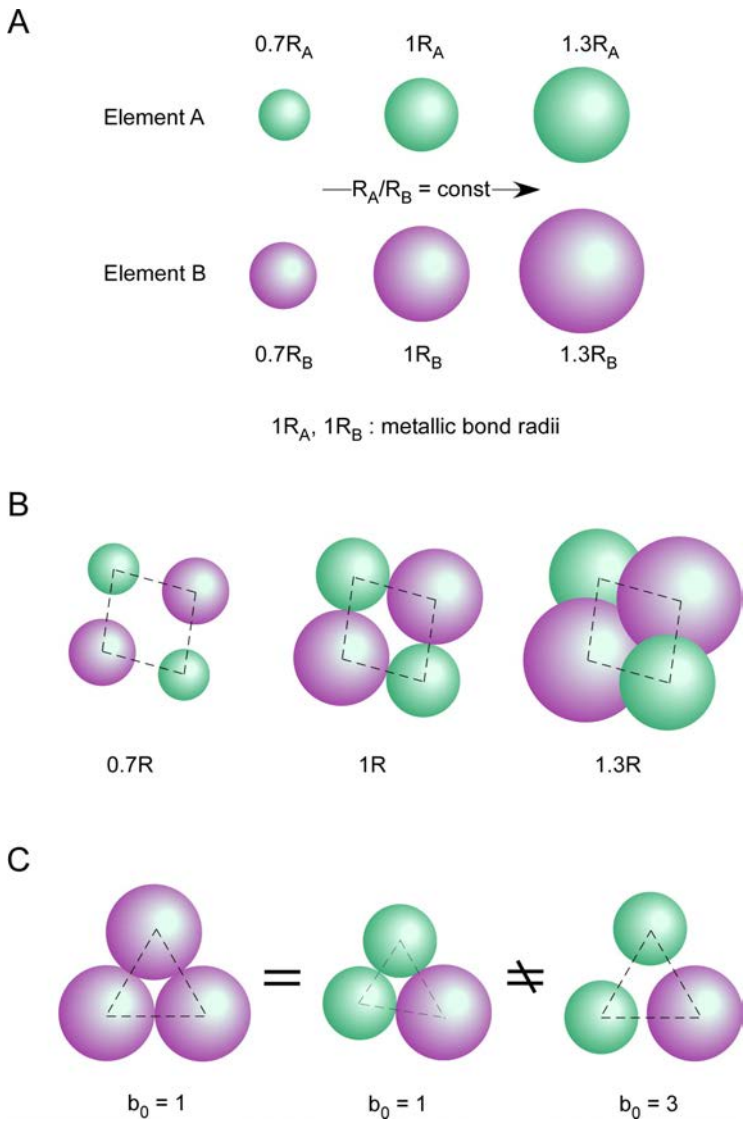


Fig. S7 Schematic diagram of the homology analysis. The atom size ratio ($R_A/R_B$) keeps a constant in the analysis (in (A)), while the atom positions are always fixed (in (B)). By changing the virtual atomic radii, we can monitor the change of the Betti number $b_0$ (number of connected components) to characterize the distortion manner of the clusters. If coordinates of each atom center are exactly identical for some atomic configurations, the size of constituent atoms affects the Betti numbers as shown in (C).

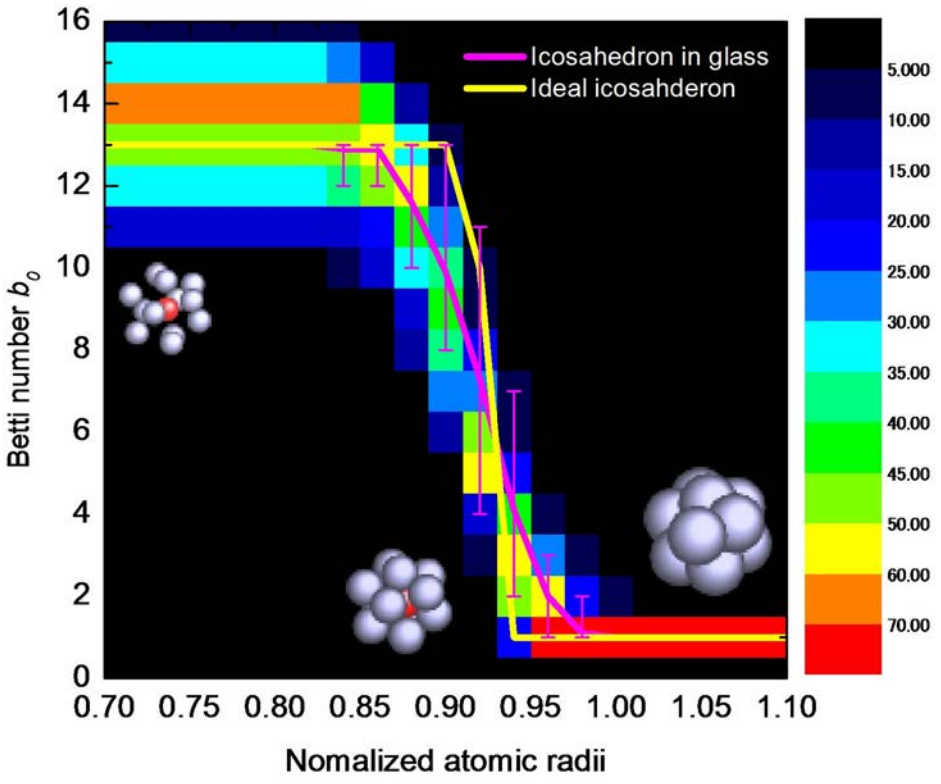


Fig. S8 Topology analysis for the distorted icosahedra (<0 0 12 0>) determined by ABED. Both ideal and distorted icosahedra are Pt centered polyhedra with 12 Zr surrounding atoms (12Zr-Pt). Error bars indicate the variation ranges of the Betti number of the distorted icosahedra. The histogram of all atomic clusters (200 clusters) in the Zr-Pt MD model is also shown. The color bar indicates the frequency of Betti number $b_0$ for each normalized atomic radii.

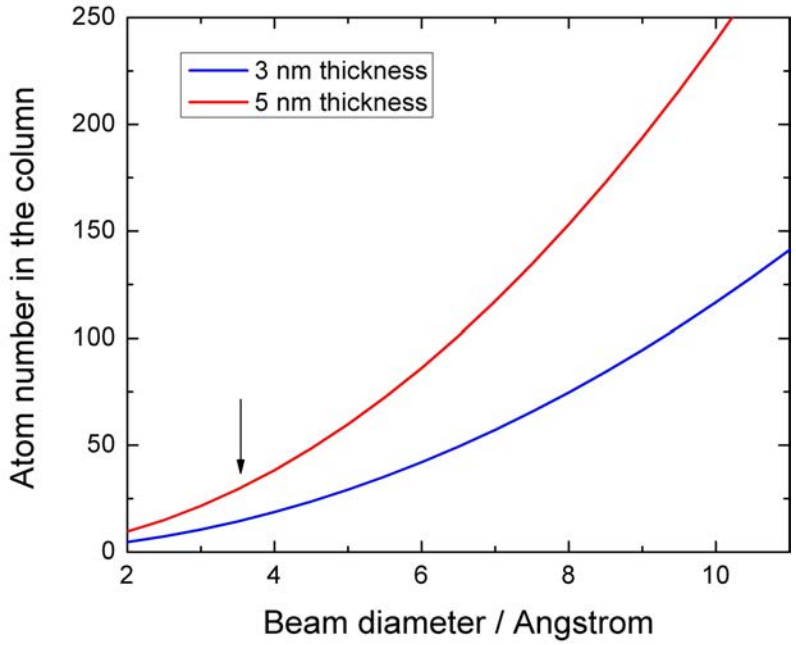


Fig. S9 Relationship between the electron beam size and the number of atoms in the columns where an electron beam passes through. The sample thicknesses are set to 3 and 5 nm, respectively. The average bond distance and packing density used in calculation are 0.30 nm and 0.7.

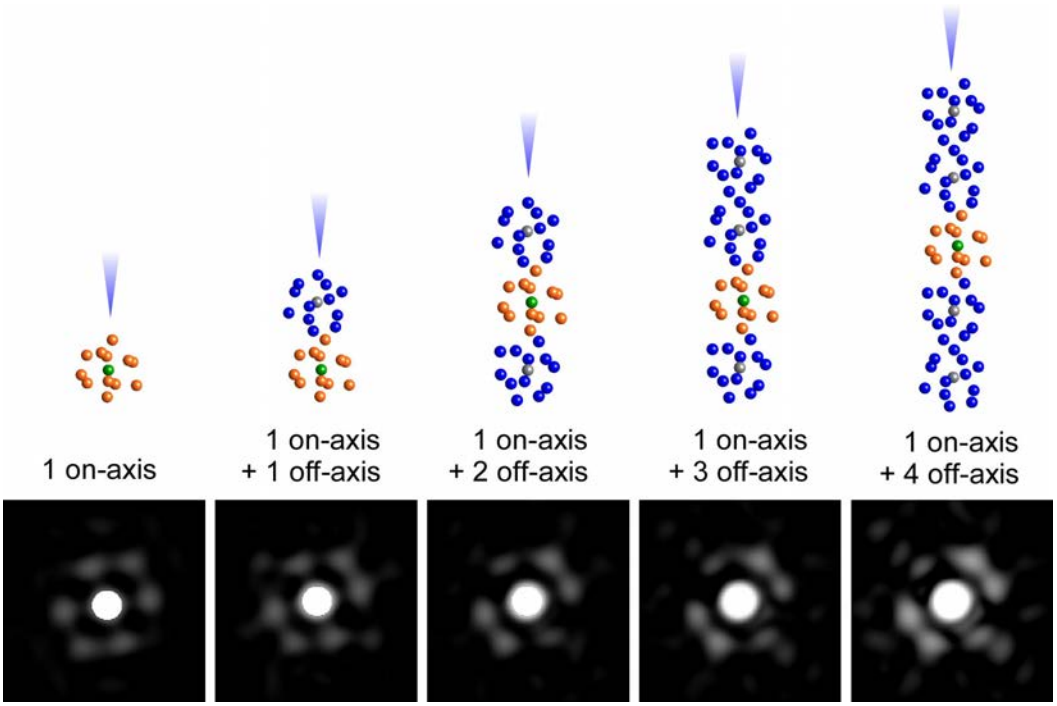


Fig. S10 Effect of the sample thickness on ABED. On-axis cluster gives the strongest intensity in the ABED patterns, whereas off-axis clusters do not contribute to the total intensity.

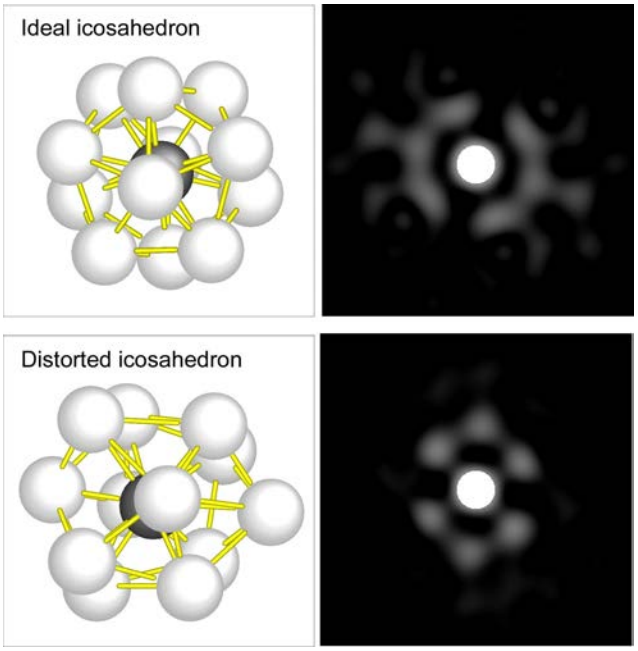


Fig. S11 Simulated ABED patterns from ideal and distorted icosahedra. The beam incidence direction is slightly tilted from the exact fivefold axes. The ideal icosahedron gives quite broad intensity, whereas the distorted one has a symmetric pattern with well-defined spots.

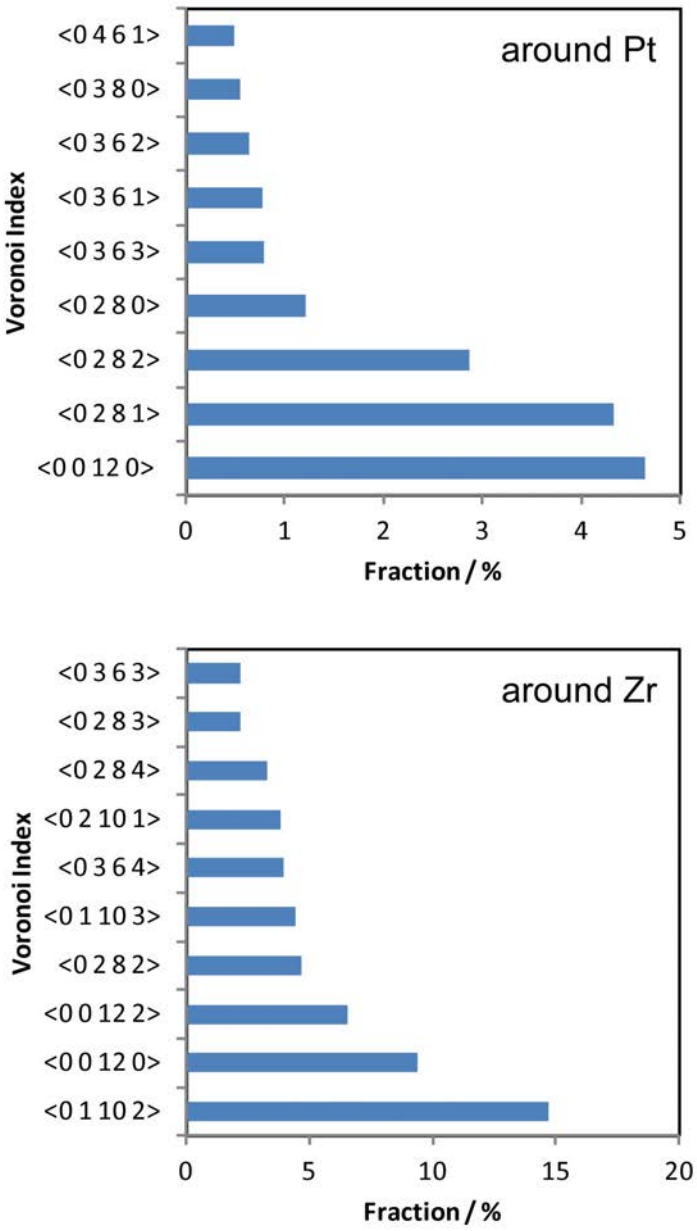


Fig. S12 Voronoi polyhedral analysis for the $Zr_{80}Pt_{20}$ taken from 12,000 atom model obtained by the classical MD simulation at the cooling rate of $1.7 \times 10^{10}$ K/sec.

**References and Notes**


1. F. C. Frank, Supercooling of liquids. *Proc. R. Soc. Lond.* **215**, 43–46 (1952). doi:10.1098/rspa.1952.0194

2. W. Hume-Rothery, E. Anderson, Eutectic compositions and liquid immiscibility in certain binary alloys. *Philos. Mag.* **5**, 383–405 (1960). doi:10.1080/14786436008235856

3. J. D. Bernal, Geometry of the structure of monatomic liquids. *Nature* **185**, 68–70 (1960). doi:10.1038/185068a0

4. G. D. Scott, Radial distribution of the random close packing of equal spheres. *Nature* **194**, 956–957 (1962). doi:10.1038/194956a0

5. J. L. Finney, Modelling the structures of amorphous metals and alloys. *Nature* **266**, 309–314 (1977). doi:10.1038/266309a0

6. P. J. Steinhardt, D. R. Nelson, M. Ronchetti, Icosahedral bond orientational order in supercooled liquids. *Phys. Rev. Lett.* **47**, 1297–1300 (1981). doi:10.1103/PhysRevLett.47.1297

7. T. Tomida, T. Egami, Molecular-dynamics study of orientational order in liquids and glasses and its relation to the glass transition. *Phys. Rev. B* **52**, 3290–3308 (1995). doi:10.1103/PhysRevB.52.3290

8. M. W. Chen, T. Zhang, A. Inoue, A. Sakai, T. Sakurai, Quasicrystals in a partially devitrified $Zr_{65}Al_{7.5}Ni_{10}Cu_{12.5}Ag_5$ bulk metallic glass. *Appl. Phys. Lett.* **75**, 1697 (1999). doi:10.1063/1.124793

9. D. B. Miracle, A structural model for metallic glasses. *Nat. Mater.* **3**, 697–702 (2004). doi:10.1038/nmat1219 Medline

10. H. W. Sheng, W. K. Luo, F. M. Alamgir, J. M. Bai, E. Ma, Atomic packing and short-to-medium-range order in metallic glasses. *Nature* **439**, 419–425 (2006). doi:10.1038/nature04421 Medline

11. P. F. Guan, T. Fujita, A. Hirata, Y. H. Liu, M. W. Chen, Structural origins of the excellent glass forming ability of $Pd_{40}Ni_{40}P_{20}$. *Phys. Rev. Lett.* **108**, 175501 (2012). doi:10.1103/PhysRevLett.108.175501 Medline

12. D. Ma, A. D. Stoica, X.-L. Wang, Power-law scaling and fractal nature of medium-range order in metallic glasses. *Nat. Mater.* **8**, 30–34 (2009). doi:10.1038/nmat2340 Medline

13. T. Takagi, T. Ohkubo, Y. Hirotsu, B. S. Murty, K. Hono, D. Shindo, Local structure of amorphous $Zr_{70}Pd_{30}$ alloy studied by electron diffraction. *Appl. Phys. Lett.* **79**, 485 (2001). doi:10.1063/1.1383055

14. A. R. Yavari, Solving the puzzle of eutectic compositions with ‘miracle glasses’. *Nat. Mater.* **4**, 2–3 (2005). doi:10.1038/nmat1289

15. J. F. Sadoc, R. Mosseri, *Geometrical Frustration* (Cambridge Univ. Press, Cambridge, 1999).

16. D. R. Nelson, *Defects and Geometry in Condensed Matter* (Cambridge Univ. Press, Cambridge, 2002).

17. D. R. Nelson, Liquids and glasses in spaces of incommensurate curvature. *Phys. Rev. Lett.* **50**, 982–985 (1983). doi:10.1103/PhysRevLett.50.982

18. A. Di Cicco, A. Trapananti, S. Faggioni, A. Filipponi, Is there icosahedral ordering in liquid and undercooled metals? *Phys. Rev. Lett.* **91**, 135505 (2003). doi:10.1103/PhysRevLett.91.135505 Medline

19. D. R. Nelson, Order, frustration, and defects in liquids and glasses. *Phys. Rev. B* **28**, 5515–5535 (1983). doi:10.1103/PhysRevB.28.5515

20. T. Schenk, D. Holland-Moritz, V. Simonet, R. Bellissent, D. M. Herlach, Icosahedral short-range order in deeply undercooled metallic melts. *Phys. Rev. Lett.* **89**, 075507 (2002). doi:10.1103/PhysRevLett.89.075507 Medline

21. K. Saksl, H. Franz, P. Jóvári, K. Klementiev, E. Welter, A. Ehnes, J. Saida, A. Inoue, J. Z. Jiang, Evidence of icosahedral short-range order in $Zr_{70}Cu_{30}$ and $Zr_{70}Cu_{29}Pd_1$ metallic glasses. *Appl. Phys. Lett.* **83**, 3924 (2003). doi:10.1063/1.1626266

22. K. F. Kelton, G. W. Lee, A. K. Gangopadhyay, R. W. Hyers, T. J. Rathz, J. R. Rogers, M. B. Robinson, D. S. Robinson, First x-ray scattering studies on electrostatically levitated metallic liquids: Demonstrated influence of local icosahedral order on the nucleation barrier. *Phys. Rev. Lett.* **90**, 195504 (2003). doi:10.1103/PhysRevLett.90.195504 Medline

23. A. Hirata, P. Guan, T. Fujita, Y. Hirotsu, A. Inoue, A. R. Yavari, T. Sakurai, M. Chen, Direct observation of local atomic order in a metallic glass. *Nat. Mater.* **10**, 28–33 (2011). doi:10.1038/nmat2897 Medline

24. N. A. Mauro, V. Wessels, J. C. Bendert, S. Klein, A. K. Gangopadhyay, M. J. Kramer, S. G. Hao, G. E. Rustan, A. Kreyssig, A. I. Goldman, K. F. Kelton, Short- and medium-range order in $Zr_{80}Pt_{20}$ liquids. *Phys. Rev. B* **83**, 184109 (2011). doi:10.1103/PhysRevB.83.184109

25. J. Saida, K. Itoh, S. Sato, M. Imafuku, T. Sanada, A. Inoue, Evaluation of the local environment for nanoscale quasicrystal formation in $Zr_{80}Pt_{20}$ glassy alloy using Voronoi analysis. *J. Phys. Condens. Matter* **21**, 375104 (2009). doi:10.1088/0953-8984/21/37/375104 Medline

26. P. J. Steinhardt, D. R. Nelson, M. Ronchetti, Bond-orientational order in liquids and glasses. *Phys. Rev. B* **28**, 784–805 (1983). doi:10.1103/PhysRevB.28.784

27. T. Egami, S. Aur, Local atomic structure of amorphous and crystalline alloys: Computer simulation. *J. Non-Cryst. Solids* **89**, 60–74 (1987). doi:10.1016/S0022-3093(87)80321-6

28. Y. Q. Cheng, E. Ma, Atomic-level structure and structure–property relationship in metallic glasses. *Prog. Mater. Sci.* **56**, 379–473 (2011). doi:10.1016/j.pmatsci.2010.12.002

29. T. Kaczynski, K. Mischaikow, M. Mrozek, *Computational Homology* (Springer, New York, 2003).

30. M. D. Ediger, P. J. Harrowell, *Chem. Phys.* **137**, 080901 (2012).

31. L. Berthier, G. Biroli, Theoretical perspective on the glass transition and amorphous materials. *Rev. Mod. Phys.* **83**, 587–645 (2011). doi:10.1103/RevModPhys.83.587

32. H. Shintani, H. Tanaka, Frustration on the way to crystallization in glass. *Nat. Phys.* **2**, 200–206 (2006). doi:10.1038/nphys235

33. G. Tarjus, S. Kivelson, Z. Nussinov, P. Viot, The frustration-based approach of supercooled liquids and the glass transition: A review and critical assessment. *J. Phys. Condens. Matter* **17**, R1143–R1182 (2005). doi:10.1088/0953-8984/17/50/R01

34. J. S. Langer, The mysterious glass transition. *Phys. Today* **60**, 8 (2007). doi:10.1063/1.2711621

35. J. A. Lin, J. M. Cowley, Calibration of the operating parameters for an HB5 stem instrument. *Ultramicroscopy* **19**, 31–42 (1986). doi:10.1016/0304-3991(86)90005-7

36. G. Kresse, J. Furthmüller, Efficiency of ab-initio total energy calculations for metals and semiconductors using a plane-wave basis set. *Comput. Mater. Sci.* **6**, 15–50 (1996). doi:10.1016/0927-0256(96)00008-0

37. P. E. Blöchl, Projector augmented-wave method. *Phys. Rev. B* **50**, 17953–17979 (1994). doi:10.1103/PhysRevB.50.17953 Medline

38. Y. Wang, J. P. Perdew, Correlation hole of the spin-polarized electron gas, with exact small-wave-vector and high-density scaling. *Phys. Rev. B* **44**, 13298–13307 (1991). doi:10.1103/PhysRevB.44.13298 Medline

39. E. J. Kirkland, *Advanced Computing in Electron Microscopy* (Plenum, New York, 1998).

40. H. Edelsbrunner, J. L. Harer, *Computational Topology: An Introduction* (American Mathematical Society, Providence, RI, 2010).